Case Studies in Thermal Engineering 49 (2023) 103307

Contents lists available at ScienceDirect

Case Studies in Thermal Engineering

journal homepage: www.elsevier.com/locate/csite

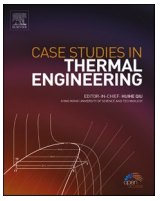

Thermo-economic assessments on building heating by a thermal energy storage system with metal foam

Xinyu Gao [a], Zhaoyang Niu [a], Xinyu Huang [a], Xiaohu Yang [a,b,*], Jinyue Yan [b,c,**]

[a] Institute of the Building Environment & Sustainability Technology, School of Human Settlements and Civil Engineering, Xi'an Jiaotong University, Xi'an, 710049, China
[b] School of Sustainable Development of Society and Technology, Mälardalen University, 72123, Västerås, Sweden
[c] Department of Building Environment and Energy Engineering, The Hong Kong Polytechnic University, Kowloon, Hong Kong, China

ARTICLE INFO

Handling Editor: Huihe Qiu

Keywords:
Thermal heat storage
Solar energy
Heating
Thermo-economic analysis

ABSTRACT

Due to the intermittency and discontinuity of solar energy, thermal energy storage (TES) using phase change materials (PCMs) is generally required to ensure stable operation in solar heating systems (SHS) during winter. This paper presents the design of a TES unit with different horizontal metal foam filling ratios (60%–100%), and simulations of thermal characteristics, such as complete melting time and heat storage capacity by numerical method. Based on the heating demands of an office building in Xi'an, TES units are combined in parallel and economic indexes are calculated based on static evaluation method, including initial investment and investment payback period. Novelty, the contribution of gradient microstructure to the phase transition process is evaluated from thermophysical properties and economy. Results show that the TES unit with a filling ratio of 90% possesses the shortest complete melting time of 5310 s, which is 87.56% shorter than that of a TES unit with pure PCM. Finally, economic assessments of the engineering application of the partially filled metal foam structure are carried out, and it is determined that the SHS with the TES system of 90% filling ratio requires the least number of 548 TES units, with a payback period of three heating seasons.

Nomenclature

Abbreviation

CPCM	Composite phase change material
HTF	Heat transfer fluid
LHS	Latent heat storage
PCM	Phase change material
PPI	Pores per inch
TES	Thermal energy storage

* Corresponding author. Institute of the Building Environment & Sustainability Technology, School of Human Settlements and Civil Engineering, Xi'an Jiaotong University, Xi'an, 710049, China.
** Corresponding author. School of Sustainable Development of Society and Technology, Mälardalen University, 72123, Västerås, Sweden.
E-mail addresses: xiaohuyang@xjtu.edu.cn (X. Yang), jinyue.yan@mdh.se (J. Yan).

https://doi.org/10.1016/j.csite.2023.103307
Received 7 March 2023; Received in revised form 17 May 2023; Accepted 15 July 2023
Available online 17 July 2023

SHS	Solar heating system

Symbols

A_m	Liquid fraction term
C_E	Inertial coefficient(m^{-1})
D	Thickness of the ligaments /mm
c_d	Drag coefficient
$c_{p,f}$	Specific heat of PCM $(\mathrm{J}\cdot\mathrm{kg}^{-1}\cdot\mathrm{K}^{-1})$
c_{ps}	Specific heat of metal foam $(\mathrm{J}\cdot\mathrm{kg}^{-1}\cdot\mathrm{K}^{-1})$
d_f	Fiber diameter (m)
d_p	Pore diameter (m)
f_m	Melting fraction
g	Gravitational acceleration $(\mathrm{m}\cdot\mathrm{s}^{-2})$
G	Shape function for metallic ligaments
H	Height (m)
h	Thickness (m)
h_{sf}	Heat transfer coefficient between internal ligament of metal foam and paraffin $(\mathrm{W}\cdot\mathrm{m}^{-1}\cdot\mathrm{K}^{-1})$
K	Permeability (m^{-2})
L	Latent heat of fusion of PCM $(\mathrm{kJ}\cdot\mathrm{kg}^{-1})$
Pr	Prandtl number
R	Radius of the heat storage tube (m)
Re	Reynolds number
t	Time (s)
T	Temperature (K)
T_{cold}	Temperature of the cold bath$(^{\circ}\mathrm{C})$
T_{hot}	Temperature of the hot bath$(^{\circ}\mathrm{C})$
T_l	Melting temperature of PCM liquid point$(^{\circ}\mathrm{C})$
T_s	Melting temperature of PCM solid point$(^{\circ}\mathrm{C})$
$\overrightarrow{U}$	Velocity vector $(\mathrm{m}\cdot\mathrm{s}^{-1})$

Greek symbols

α	Filling ratio of metal foam
α_{sf}	Specific area (m^{-1})
γ	Thermal expansion coefficient (K^{-1})
δ	Numerical constant
$10^{-4}\varepsilon$	Porosity
ς	Dimensionless thickness of the node for the metal foam
λ_{fe}	Thermal conductivity of paraffin $(\mathrm{W}\cdot\mathrm{m}^{-1}\cdot\mathrm{K}^{-1})$
λ_{se}	Effective thermal conductivity of metal foam$(\mathrm{W}\cdot\mathrm{m}^{-1}\cdot\mathrm{K}^{-1})$
μ_l	Dynamic viscosity of paraffin$(\mathrm{kg}\cdot\mathrm{m}^{-1}\cdot\mathrm{s}^{-1})$
ξ	Dimensionless surface area of the node for the metal foam
ρ_l	Density of paraffin $(\mathrm{kg}\cdot\mathrm{m}^{-3})$
ρ_s	Density of metal foam $(\mathrm{kg}\cdot\mathrm{m}^{-3})$
σ	Liquid fraction liquid in the metal foam
ψ	Paste zone coefficient, take 10^8
χ	Flow tortuosity
ω	Pore density

Subscript

f	*PCM in fluid phase*
fe	*Paraffin*
m	*Melting*
s	*PCM in solid phase*
se	*Metal foam*

1. Introduction

With the excessive depletion of fossil energy resources, there is an increasing focus on exploring and utilizing renewable energy sources. The continuously rising energy consumption of buildings is having a serious impact on the environment [1]. To protect the ecological environment and promote sustainable development, it is crucial to quest for alternative fuels without depending on fossil energy. Solar energy, as a representative renewable energy, can be utilized for winter heating to address the energy problems of buildings [2]. However, due to the intermittency and discontinuity of solar energy, thermal energy storage (TES) system is requisite to ensure the stability application in many practical projects [3]. There are three feasible TES approaches: sensible heat storage, latent heat storage and chemical heat storage [4–6]. Among them, latent heat storage (LHS) with phase change materials (PCMs) can store a large amount of thermal energy with minimal temperature fluctuations, and the temperature of supply and return water offered by the LHS system is suitable for central heating [7,8]. As a result, LHS with PCMs is widely employed in solar heating system (SHS) for buildings.

SHS with TES not only plays a crucial role in bridging the gap between supply and demand, but also can overcome the hysteresis of heating pipe network [9–12]. A number of studies have analyzed the thermophysical properties of TES system and evaluated the feasibility of their applications in SHS. Zhao et al. [13] explored the difference between SHS with PCM and SHS without PCM, and the results indicated that the energy consumption of SHS without PCM was 34% more than the energy consumption of SHS with PCM. Yang et al. [14] conducted a sensitivity analysis of the district heating plant and found that the system with seasonal thermal storage was feasible when considering the unit prices of the solar thermal collectors system and seasonal thermal storage device, as well as the solar fraction. Ushamah et al. [15] conducted a study on the thermal and economic characteristics of solar heating systems with TES systems and identified the optimal solar thermal utilization technology. Meanwhile, Mathew et al. [16] experimentally investigated a solar air heater with heat storage medium (Therminol 55) appropriate for high-temperature and estimated the payback period for the device at 69 months.

Despite the significant potential of thermal energy storage (TES) systems in sustainable heating systems (SHS), the thermal storage efficiency of engineering PCMs remains extremely low, limiting their widespread application. Previous studies have demonstrated that the addition of high thermal conductivity materials can enhance the performance of PCMs. These materials include, but are not limited to metal fins [17–20], nanofluids [21–24], microcapsules [25–27], heat pipes [28–31], and composite structure of them [32,33]. Liu et al. [33] conducted experimental research on the thermal characteristics of PCM (paraffin) when combined with metal fins, metal foam, and a hybrid of both. The study revealed that the hybrid structure was the most effective, and the full phase transition time was decreased by 63.4% compared to pure PCM. In contrast, Walter et al. [34] numerically investigated the charging/discharging process of transverse and longitudinal bifurcated finned tubes. The study found that the transverse fins hindered the charging/discharging speed due to the physical barrier they created.

In academic discourse, it is commonly acknowledged that metal foam with a high porosity level is an effective approach to improving heat transfer due to its porous structure, as evidenced by previous research [35–41]. However, given the high cost of metal foam, reducing the amount of filling is necessary to minimize the initial investment. Therefore, it is essential to establish a balance between economic considerations and the desired level of efficiency. To enhance the heat storage capability and minimize the investment cost of thermal energy storage (TES) units, scholars have conducted studies aimed at determining the optimal structure of phase change materials (PCMs) filled with metal foam [42–49]. Zhang et al. [50] investigated the use of linear gradient aluminum foam as a filling material for PCMs and found that this structure significantly improved the efficiency of the phase transition process. Karimi et al. [51] designed a helical coil and porous foamed metal structure to enhance the efficiency of latent heat TES. The experimental results indicated that the application of metal foam significantly decreased the melting/solidification time by up to 57%. In a numerical simulation of the porosity combination of metal foam, Wang et al. [52] concluded that the porosity combination of 0.97–0.890 exhibited superior thermophysical properties when compared to other combinations. Recently, some scholars have investigated the flow, heat transfer and melting properties of PCM in metal foams based on pore-scale analysis [53]. Paknahad et al. [54] established decoupled lattice Boltzmann solver to simulate advection-diffusion in the non-Darcy regime, and explored pore-scale flow and conjugate heat transfer in metallic foams with various porosity and density. Hu et al. [55] conducted a pore-scale numerical simulation to explain the influence of porosity and pore density, it indicated that the melting efficiency of low porosity and high pore density structure was higher than that of high porosity and low pore density structure.

Prior research has predominantly focused on uniform parameters in the optimization of heat storage with metal foam, indicating a need for further exploration of optimal metal foam structures. The thermophysical properties of horizontal partially filled metal foam structures in heat accumulators remain uncertain. Furthermore, there is a lack of economic analysis regarding the optimization of partially filled metal foam structures in thermal energy storage (TES) systems. This study aims to investigate the thermophysical characteristics of partially filled metal foam thermal energy storage (TES) units, specifically focusing on the complete melting time and heat storage capacity. The study utilizes an office building located in Xi'an as a case study, whereby the designed TES units are combined in parallel to meet the building's heating demand. The investment costs and payback periods of various filling ratios are calculated and compared to evaluate the economic feasibility of utilizing partially filled metal foam structures in engineering applications.

2. Numerical models for heat storage and release

2.1. Model description

Fig. 1(a) illustrates the operating principle of the solar heating system (SHS) with thermal energy storage (TES). The shell-and-tube TES system is designed to utilize the unique material characteristics of phase change materials (PCMs) to store solar heat energy as they

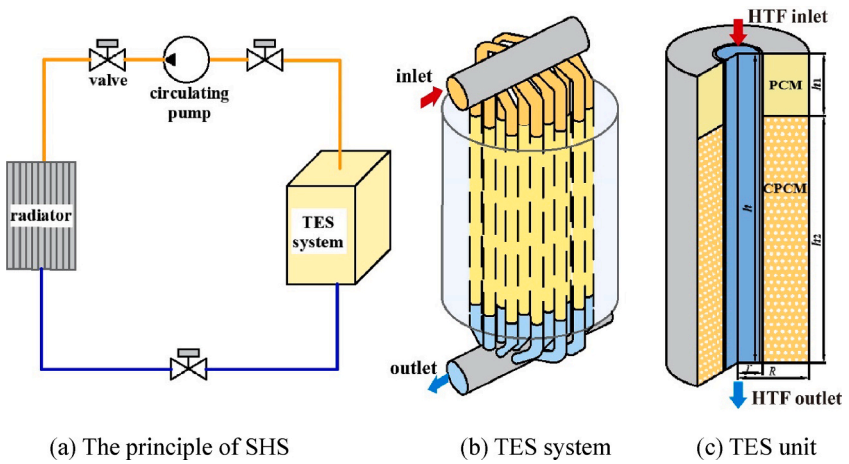

Fig. 1. Physical model of horizontal partially filled TES unit.

transition from a solid to a liquid state. As the PCM undergoes this transition, latent heat is released and can be utilized for heating purposes. To meet the heating demand of thermal users, the heat transfer fluid (HTF) is heated by the TES system and circulated to the radiator via a circulating pump. Ultimately, the TES system ensures that the absorbed solar energy is effectively utilized to meet the thermal needs of end-users. The TES system is primarily comprised of multigroup TES units arranged in parallel configuration, as depicted in Fig. 1(b). In this system, the heat transfer fluid (HTF) flows through the side of tube, while the shell side is filled with phase change material (PCM) and partially filled with horizontally oriented metal foam. As a single TES unit can typically demonstrate the thermal behavior of the entire shell-and-tube TES system, the present study establishes a TES unit to investigate the thermophysical characteristics of the system, as illustrated in Fig. 1(c). The height (h) of the concentric cylinder, as well as the inner (r) and outer (R) diameters of the HTF tube (copper tube), are 270 mm, 22 mm, and 90 mm, respectively. Meanwhile, the wall thickness of the HTF tube is 1 mm. Additionally, the horizontal partially filling ratio (α) of the metal foam is defined as the ratio of heights (h_1/h_2) between the pure PCM region and the composite phase change material embedded with metal foam (CPCM) region when the upper surface is horizontal. Ten structures with different filling ratios are considered in this paper, as exhibited in Table 1.

2.2. Governing equations

Continuity equation:

$$\frac{\partial \rho_l}{\partial t}+\nabla\left(\rho_l\langle\vec{U}\rangle\right)=0 \tag{1}$$

Momentum equation:

X-direction:

$$\frac{\rho_l}{\sigma}\frac{\partial\langle u\rangle}{\partial t}+\frac{\rho_l}{\sigma^2}\left(\langle\vec{U}\rangle\cdot\nabla\right)\langle u\rangle=-\frac{\partial\langle P\rangle}{\partial x}+\frac{\mu_l}{\sigma}\nabla^2\langle u\rangle-\left(\frac{\mu_l}{K}+\frac{\rho_l C_E}{\sqrt{K}}\left|\langle\vec{U}\rangle\right|\right)\langle u\rangle -\frac{(1-f_{\mathrm{m}})^2}{{f_{\mathrm{m}}}^3+\delta}A_m\langle u\rangle+\rho_f g\gamma\left(\langle T_f\rangle-T_{m1}\right) \tag{2}$$

y-direction:

$$\frac{\rho_l}{\sigma}\frac{\partial\langle v\rangle}{\partial t}+\frac{\rho_l}{\sigma^2}\left(\langle\vec{U}\rangle\cdot\nabla\right)\langle v\rangle=-\frac{\partial\langle P\rangle}{\partial x}+\frac{\mu_l}{\sigma}\nabla^2\langle v\rangle-\left(\frac{\mu_l}{K}+\frac{\rho_l C_E}{\sqrt{K}}\left|\langle\vec{U}\rangle\right|\right)\langle v\rangle -\frac{(1-f_{\mathrm{m}})^2}{{f_{\mathrm{m}}}^3+\delta}A_m\langle v\rangle+\rho_f g\gamma\left(\langle T_f\rangle-T_{m1}\right) \tag{3}$$

Table 1
Ten structures of horizontal partially filled TES units.

Case	Filling ratio	Case	Filling ratio
1	0%	6	80%
2	60%	7	85%
3	65%	8	90%
4	70%	9	95%
5	75%	10	100%

z-direction:

$$\frac{\rho_l}{\sigma}\frac{\partial\langle w\rangle}{\partial t}+\frac{\rho_l}{\sigma^2}\left(\langle\vec{U}\rangle\cdot\nabla\right)\langle w\rangle=-\frac{\partial\langle P\rangle}{\partial z}+\frac{\mu_l}{\sigma}\nabla^2\langle w\rangle-\left(\frac{\mu_l}{K}+\frac{\rho_l C_E}{\sqrt{K}}\left|\langle\vec{U}\rangle\right|\right)\langle w\rangle -\frac{(1-f_{\mathrm{m}})^2}{f_{\mathrm{m}}{}^3+\delta}A_m\langle w\rangle+\rho_f g\gamma\left(\langle T_f\rangle-T_{m1}\right) \tag{4}$$

Energy equation for PCM:

$$\varepsilon\rho_f\left(c_{p,f}+L\frac{\mathrm{d}f_{\mathrm{m}}}{\mathrm{d}T_f}\right)\frac{\partial\langle T_f\rangle}{\partial t}+\rho_f c_{p,f}\langle\vec{U}\cdot\nabla\rangle\langle T_f\rangle=\nabla^2\left(\lambda_{fe}+\lambda_{td}\right)\langle T_f\rangle-h_{sf}a_{sf}\left(\langle T_l\rangle-\langle T_s\rangle\right) \tag{5}$$

Energy equation for metal foam:

$$(1-\varepsilon)\rho_s c_{ps}\frac{\partial\langle T_s\rangle}{\partial t}=\nabla\cdot\left(\lambda_{se}\nabla\langle T_s\rangle\right)-h_{sf}a_{sf}\left(\langle T_s\rangle-\langle T_f\rangle\right) \tag{6}$$

where represents the volume average; σ donates the liquid fraction in metal foam, ($\sigma=\varepsilon f_f$); ρ_l, μ_l, γ, $c_{p,f}$, λ_{td}, λ_{fe} and L define separately density, dynamic viscosity, thermal expansion coefficient, specific heat, thermal dispersion coefficient, thermal conductivity and latent heat for PCM; ρ_s, c_{ps}, λ_{se}, K, C_E, ε and a_{sf} are the density, specific heat, effective thermal conductivity, permeability, inertia coefficient, porosity, and specific surface area of metal foam, respectively. The Forchheimer-Darcy term $\left(\frac{\mu_f}{K}+\frac{\rho_f C_E}{\sqrt{K}}\left|\langle\vec{U}\rangle\right|\right)\langle u\rangle$ is employed to reflect flow resistance in the porous medium. $\frac{(1-f_{\mathrm{m}})^2}{f_{\mathrm{m}}{}^3+\delta}A_m$ is used to donate the phase change.

The melting fraction f_m is defined as:

$$f_m=\begin{cases}0T<T_{m1}\\ \dfrac{T-T_{m1}}{T_{m2}-T_{m1}}T_{m1}\le T\le T_{m2}\\ 1T>T_{m2}\end{cases} \tag{7}$$

where δ and A_m are the empirical constant ($\delta=10^{-4}$) and paste zone coefficient ($A_m=10^5$), respectively. When $f_{\mathrm{m}}=0$, A_m approaches infinity, and the value of δ ensures that the denominator is not zero.

The heat transfer coefficienth_{sf} is calculated by Ref. [56]:

$$h_{sf}=\begin{cases}0.76\mathrm{Re}^{0.4}\,\mathrm{Pr}^{0.37}\lambda_f/D, 0<\mathrm{Re}\le 40\\ 0.52\mathrm{Re}^{0.5}\,\mathrm{Pr}^{0.37}\lambda_f/D, 40<\mathrm{Re}\le 1000\\ 0.26\mathrm{Re}^{0.6}\,\mathrm{Pr}^{0.37}\lambda_f/D, 1000<\mathrm{Re}\le 20000\end{cases} \tag{8}$$

Effective thermal conductivityλ_e is defined as [57]:

$$\frac{\lambda_e}{\lambda_{lig}}=\frac{(1-\varepsilon)}{\left(1-\varsigma+\frac{3\varsigma}{2\xi}\right)\left[3(1-\varsigma)+\frac{3}{2}\xi\varsigma\right]}+\frac{\lambda_l}{\lambda_{lig}}\varepsilon \tag{9}$$

where ς and ξ represent the dimensionless thickness and the dimensionless surface area of the node for the metal foam, in respective.

Thermal dispersion conductivity λ_{td} is determined by Ref. [58]:

Table 2
Thermophysical properties of materials.

Material	Variable	Value
Paraffin	Density ($\mathrm{kg\cdot m^{-3}}$)	850 (solid)/800 (liquid)
	Specific heat capacity ($\mathrm{J\cdot kg^{-1}\cdot K^{-1}}$)	2000
	Thermal conductivity ($\mathrm{W\cdot m^{-1}\cdot K^{-1}}$)	0.2 (solid)/0.1 (liquid)
	Latent heat of fusion ($\mathrm{kJ\cdot kg^{-1}}$)	200
	Melting temperature range (°C)	53–54
	Thermal expansion coefficient ($\mathrm{K^{-1}}$)	7.5×10^{-4}
	Dynamic viscosity ($\mathrm{kg\cdot m^{-1}\cdot s^{-1}}$)	2.51×10^{-3}
Water	Density ($\mathrm{kg\cdot m^{-3}}$)	998.2
	Specific heat capacity ($\mathrm{J\cdot kg^{-1}\cdot K^{-1}}$)	4182
	Dynamic viscosity ($\mathrm{kg\cdot m^{-1}\cdot s^{-1}}$)	1.003×10^{-3}
	Thermal conductivity ($\mathrm{W\cdot m^{-1}\cdot K^{-1}}$)	0.6
Copper	Density ($\mathrm{kg\cdot m^{-3}}$)	8920
	Specific heat capacity ($\mathrm{J\cdot kg^{-1}\cdot K^{-1}}$)	380
	Thermal conductivity ($\mathrm{W\cdot m^{-1}\cdot K^{-1}}$)	401

Table 3
Independence test of TES unit.

Mesh	Total time	Time step	Total time
15,038	5400 s	0.05 s	5330 s
42,672	5310 s	0.1 s	5310 s
1,621,629	5330 s	0.3 s	5320 s

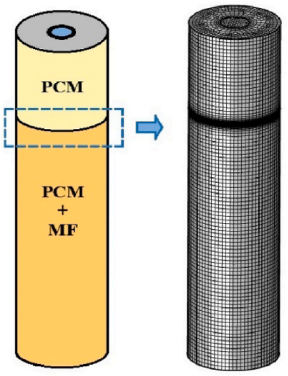

(a) Computational model meshing

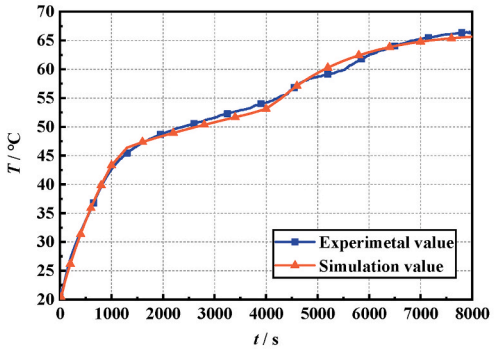

(b) Temperature comparison between numerical and experimental temperature

Fig. 2. Computational model meshing and numerical verification.

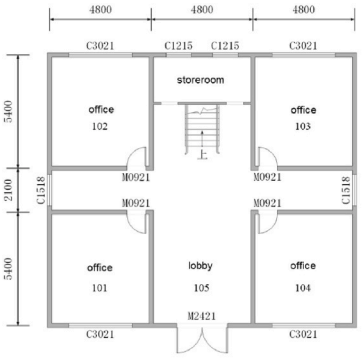

(a) Architectural plan

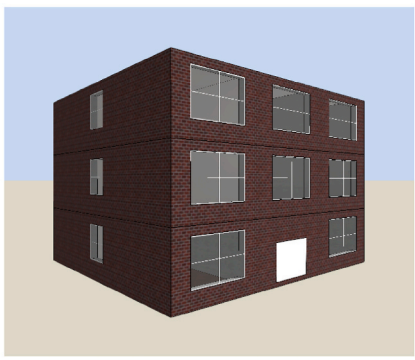

(b) Building model

Fig. 3. Building structure.

$$\lambda_{td} = \frac{0.36}{1-\varepsilon}\rho_f c_{pf} D\sqrt{u^2+v^2+w^2} \tag{10}$$

Permeability K is:

$$K = \frac{\varepsilon\left[1-(1-\varepsilon)^{1/3}\right]}{108\left[(1-\varepsilon)^{1/3}-(1-\varepsilon)\right]} {d_p}^2 \tag{11}$$

Inertial coefficient C_E is [58]:

$$C_E = 0.095\frac{c_d}{12}\sqrt{\frac{\varepsilon}{3(\chi-1)}}\left(1.18\sqrt{\frac{1-\varepsilon}{3\pi}}\ \frac{1}{G}\right)^{-1} \tag{12}$$

where c_d is the resistance coefficient ($c_d = 1.56$ [59]), χ denotes the tortuosity, and G presents the shape factor [60] :

$$\chi = \frac{\varepsilon}{1-(1-\varepsilon)^{1/3}} \tag{13}$$

$$G = 1 - e^{-(1-\varepsilon)/0.04} \tag{14}$$

2.3. Numerical settings

The physical parameters of the model material include the use of RT54 paraffin as the PCM, metal foam with a porosity of 0.94 and pore density of 15PPI as the porous material to enhance heat transfer, and water as the HTF. Table 2 provides the thermal physical parameters of the material. After importing the grid into Ansys-Fluent 18.2, the following assumptions are exhibited in the simulation model to simplify the calculation.

(1) The foamed metal is regarded as isotropic and uniformly filled.
(2) Melting paraffin is defined as isotropic and incompressible, following Boussinesq hypothesis.
(3) The volume variation in phase change process is not taken into account.
(4) It is assumed that the heat transfer between the model and the external environment is adiabatic and that the thermal contact resistance between the components of the model is zero.

Meanwhile, the governing equation of transient heat and mass transfer involving phase transition and moving boundary is solved using the finite volume method. The PISO algorithm is utilized to calculate the pressure and velocity coupling effects of forced convection in HTF and local natural convection in molten paraffin. The PRESTO! format is employed for pressure correction of the fluid in these two regions, and other physical quantities are discretized by the second-order upwind method. The relaxation factors of momentum, pressure correction, energy and liquid fraction are setting as 0.6, 0.3, 0.8 and 0.7 for assembling the convergence of continuity, momentum and energy equations (10^{-6}, 10^{-6} and 10^{-8}).

To ensure that these cases have the same initial conditions, the initial temperature for all zones is set to 22 °C and the temperature of the HTF injected from the top of the copper tube at a velocity of 0.04 m/s to 70 °C is initialized. Here are the boundary conditions.

(1) “Velocity-Inlet” is selected as the type of HTF inlet, and the HTF is 70 °C with a speed of 0.04 m/s.
(2) “Pressure-outlet” is chosen as the HTF outlet with the pressure at 1 atm.
(3) The walls close to paraffin and HTF are regarded as coupled heat transfer conditions.
(4) Other walls are considered adiabatic.

2.4. Verification of grid and time step dependence

The computational domain of the model was discretized using ANSYS-ICEM 18.2, and the mesh was generated at the boundaries of the geometric shape, the fluid-pipe wall interface, and the PCM-CPCM interface. The melting time of three groups of PCMs was compared with mesh densities of 15,038, 42,672, and 75,208 under the condition that the metal foam filling ratio of the TES unit was 90%. The difference between the complete melting time of 42,672 and 15,038 was found to be 0.37% and 1.3%, respectively, when compared with 1,621,629. Additionally, time steps of 0.3 s, 0.1 s, and 0.05 s were verified, and it was observed that the difference in complete melting time between the conditions with time steps of 0.3 s and 0.1 s and 0.05 s was less than 0.4%. These results reveal that a grid of 42,672 and a time step of 0.1 s can ensure simulation accuracy while also saving computational expenses.

Table 4
The heat transfer coefficients of building envelope.

building envelope	external wall	external window	partition	internal door	roof	floor	external door
heat transfer coefficient /W·m^{-2}·K^{-1}	0.45	2.2	1.5	2.3	0.4	0.6	1.7

Table 5
Hourly design parameters of each index.

index	indoor temperature of the heating area		room occupancy rate		utilization rate of electrical equipment		utilization rate of lighting equipment	
time	workday	holiday	workday	holiday	workday	holiday	workday	holiday
0	5	5	0	0	0	0	0	0
1	5	5	0	0	0	0	0	0
2	5	5	0	0	0	0	0	0
3	5	5	0	0	0	0	0	0
4	5	5	0	0	0	0	0	0
5	5	5	0	0	0	0	0	0
6	12	5	0	0	0	0	0	0
7	18	5	10	0	10	0	10	0
8	20	5	50	0	50	0	50	0
9	20	5	95	0	95	0	95	0
10	20	5	95	0	95	0	95	0
11	20	5	95	0	95	0	95	0
12	20	5	80	0	50	0	80	0
13	20	5	80	0	50	0	80	0
14	20	5	95	0	95	0	95	0
15	20	5	95	0	95	0	95	0
16	20	5	95	0	95	0	95	0
17	20	5	95	0	95	0	95	0
18	20	5	30	0	30	0	30	0
19	18	5	30	0	30	0	30	0
20	12	5	0	0	0	0	0	0
21	5	5	0	0	0	0	0	0
22	5	5	0	0	0	0	0	0
23	5	5	0	0	0	0	0	0

2.5. Verification of numerical model

To compare the numerical results of case 5 (filling ratio 100%) with the corresponding experiment, the measuring point is selected (125 mm from the bottom and 50 mm from the center of TES unit) and the difference is demonstrated in Fig. 2(b). The results reveals that the temperature variation tendency is consistent between the simulation and experiment process, and the maximum deviation is 1.59 °C, which confirms the rationality and accuracy of the simulations (see Fig. 3).

3. Heat load simulation

3.1. Research object

The engineering application economy of a partially filled metal foam TES system is analyzed using an office building located in Xi'an as a case study. The office building comprises of three floors, each with a height of 3.3 m. The building structure of the first floor is illustrated in Fig. 2, and the offices on the second and third floors measure 5.4 m × 4.8 m directly above the lobby on the first floor. This public building has a shape coefficient of 0.39. The hourly heat load during the heating period is simulated using Energyplus 9.3.0 software (see Table 3).

3.2. Design parameters

The indoor and outdoor design parameters of the office building are acquired in accordance with "Design Code for Heating, Ventilation and Air Conditioning of Civil Buildings" GB50736-2016. The outdoor design temperature of Xi'an is −3.4 °C, and the indoor design temperature of the offices and lobbies during winter is 20 °C. It is assumed that the office building is occupied from 7:00 to 19:00, and on-duty heating is set during the night and on holidays to maintain the indoor temperature not lower than 5 °C. The heating of the stairwell and storage room is excluded from this study. The thermal parameters of the building envelope are determined based on the thermal performance limits of Class A public buildings in cold areas specified in "Design Standard for Energy Efficiency of Public Buildings" GB50189-2015, as presented in Table 4. The heat transfer coefficient of the ground is defined through the zone division method.

In addition to establishing the thermal parameters of the building envelope, it is crucial to ensure that the hourly parameters are accurately defined, including indoor design temperature, room occupancy rate, and service time of electrical and lighting equipment. The hourly parameters for this office are presented in Table 5. Moreover, the per capita fresh air volume, the per capita building area, the power density of electrical equipment, and the illumination of lighting equipment are 8.33 L s^{-1}, 10 m^2, 15 W m^{-2}, and 200 lx, respectively. The activity intensity is classified as light physical activity. Based on the per capita fresh air volume, personnel density, and building volume, the air exchange rate is calculated to be 0.634 ac·h^{-1}. Personnel activities, lighting, and electrical heating in the building are incorporated in the room heating along with solar heat, thereby influencing the hourly heat load of the building.

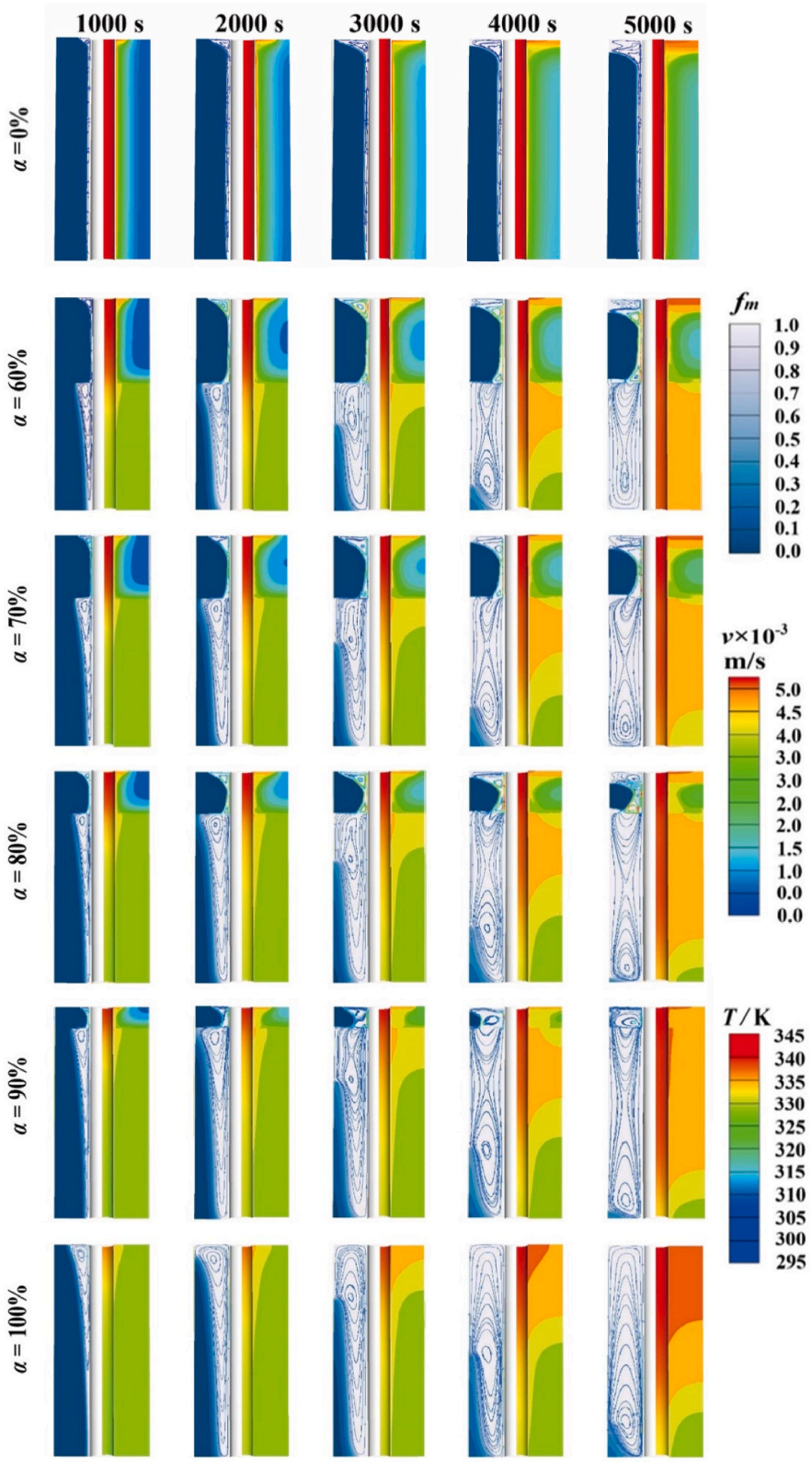

Fig. 4. The phase interface contour, temperature contour and streamline of the melting process of different ratio.

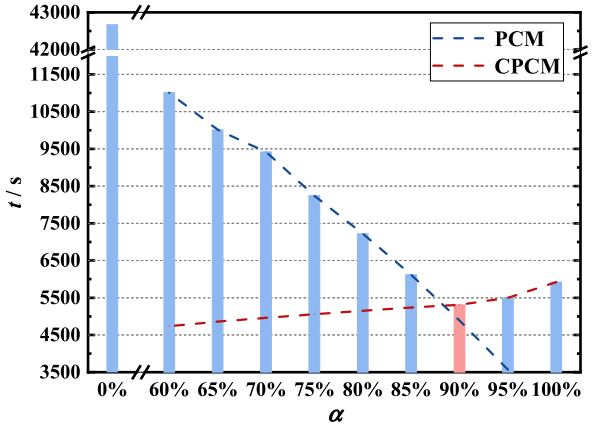

Fig. 5. Complete melting time of phase transition region with various filling ratio.

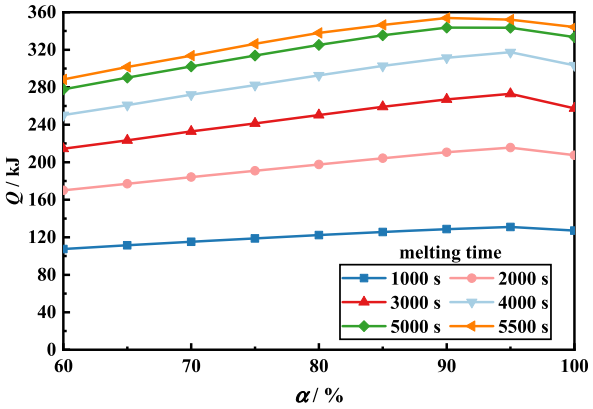

Fig. 6. Variation of paraffin heat storage with filling ratio at different melting time.

4. Results and discussion

4.1. Melting characters

To provide a more intuitive display of the melting characteristics of thermal energy storage (TES) units with varying filling ratios, Fig. 4 presents the phase interface contour, temperature contour, and streamline of TES units with 0%, 60%, 70%, 80%, 90%, and 100% filling ratios within 5000 s. In general, the addition of metal foam enhanced the heat transfer efficiency to a great extent. Regarding the phase interface, the vertical transfer of heat to the phase change material (PCM) at the bottom occurs uniformly under

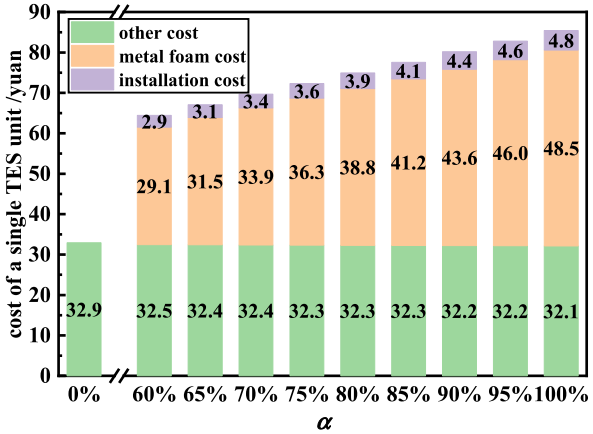

Fig. 7. Variation of the cost of a single TES unit with different filling ratio.

the influence of the metal foam, and the solid-liquid phase interface smoothly continues when the PCM is filled with metal foam. Overall, the phase interface exhibits a sudden transition or even a fractured surface at the PCM and composite phase change material (CPCM) junction. This is primarily due to the different dominant heat transfer modes in the PCM and CPCM regions, leading to distinct phase interface shapes. The volume of solid paraffin in the PCM region decreases as the filling ratio increases, while in the CPCM region, it increases. This phenomenon supports the notion that the partially filled metal foam structure accelerates the location distribution of paraffin during the melting process.

The proposed structure effectively separates the original melting region into two parts and significantly increases the contact surface area between the unmelted and melted paraffin, thereby providing a solid foundation for natural convection to enhance heat transfer. In contrast, the TES unit with a filling ratio higher than 90% completely melts the paraffin at the top after 5000 s, leaving a small amount of solid paraffin at the bottom. As the filling ratio decreases to 80% or below, the melting rate of the bottom paraffin gradually increases with the filling ratio, while the top paraffin exhibits the opposite trend. Therefore, the PCM and CPCM regions reach equilibrium when the filling ratio is 90%, which is beneficial for efficient thermal energy storage completion.

Regarding the temperature field, a significant difference between the PCM and CPCM regions is observed. The PCM region exhibits a large temperature gradient, with a local temperature difference of up to 18 K at 1000 s. The temperature of the PCM close to the inner wall is higher, reaching up to 318 K, while the temperature gradually decreases from the inner wall to the outer wall, reaching 300 K. In contrast, the temperature field in the CPCM region is relatively uniform, and the temperature in all regions with different filling ratios is higher than 334 K. This indicates that the heat transfer fluid (HTF) has difficulty in transferring heat to the PCM due to the low thermal conductivity of pure paraffin. By utilizing the high thermal conductivity of metal foam, the HTF heat can be uniformly transferred to the CPCM. From 2000 s to 5000 s, a significant temperature gradient can still be observed in the PCM region, whereas the temperature in the CPCM region gradually increases from bottom to top because of the influence of gravity. These results suggest that the partially filled metal foam facilitates the melting of paraffin in the PCM region by utilizing the melted paraffin at the top of the CPCM region.

Typically, the flow velocity in the CPCM region is relatively low, measuring less than 5×10^{-4} m/s. Conversely, the flow velocity in the PCM region can reach up to 5×10^{-3} m/s, which is an order of magnitude greater than that in the CPCM region. In the PCM region, vigorous eddies are present between the unmelted paraffin and wall surfaces, which play a crucial role in the evolution of the phase interface. As the filling ratio increases, the effect of natural convection in the melting area gradually diminishes. By combining heat conduction with the enhanced heat transfer effect of local natural convection, the TES unit with a filling ratio of 90% exhibits outstanding melting characteristics.

4.2. Thermal assessments

4.2.1. Complete melting time

Based on the simulation results, the complete melting time of pure PCM is significantly lengthy, measuring 42,670 s, rendering it impractical for real-world applications. Thus, the heat transfer should be strengthened in the PCM region. Fig. 5 illustrates the complete melting time of PCM at various filling ratios, where dashed lines represent the complete melting time of PCM and CPCM regions respectively. The complete melting time of the TES unit is dependent on the final melting part after dividing the phase transition region as demonstrated in the bar chart. As the filling ratio reduces from 100% to 60%, the phase transition time of the CPCM decreases gradually, while the melting time of the PCM region increases rapidly. This outcome can be attributed to the heat conduction that primarily relies on the convection heat transfer after the melting of the paraffin close to the copper tube wall in the PCM region. At this point, the metal foam filled at the lower part of the TES unit becomes the secondary heat source, supplying energy for the melted paraffin to travel upwards.

As the filling ratio of metal foam increases, the amount of pure PCM decreases, while the secondary heating surface moves further away, leading to a slow melting of the paraffin core. In the porous metal composite phase transition region, the foam skeleton enhances the thermal conductivity, while the foam pores limit the convection, thereby promoting the solid-liquid phase interface to mainly develop along the radial direction. Consequently, the effect of the axial filling height variation on the melting time in this region is limited. In conclusion, the optimal filling ratio of the TES unit is 90%, which leads to the fastest melting rate in the phase transition zone.

4.2.2. Heat storage capacity

Fig. 6 presents a graphical representation of the variation in paraffin heat storage for different filling ratios and melting times, which consist of both latent and sensible heat. As the melting time increases, the heat storage of the TES unit increases continuously, and the differences between different filling ratios become more evident. The optimal heat storage efficiency is achieved at filling ratios of 95% and 90%, with the heat storage of the former being higher before 4000s, while that of the latter is higher after 4000s. The results indicate that the highest heat storage efficiency is observed at filling ratios of 85% and 100%, followed by those below 80%. At 5500s, the heat storage of filling ratios 95% and 90% increased by approximately 5% compared to that of filling ratio 100%. However, as the filling ratio of the metal foam decreases from 90% to 60%, the thermal energy storage process slows down gradually, suggesting that both excessive and insufficient filling amounts of metal foam have a disadvantageous effect on the thermal energy storage of PCM.

4.3. Economic analysis of the TES system

4.3.1. Calculation of initial investment and operating cost

The initial investment required for implementing a partially filled porous metal accumulator in a building heating system is primarily composed of material cost, I_m, and installation cost, I_w. The material cost involves expenditures on paraffin, metal foam, and

pipe fitting shell. For the phase change accumulator with varying filling ratios, the dimensions of the HTF pipe and the shell of the phase change area remain constant, and the device cost is 20 yuan per unit. The volume of paraffin and metal foam is dependent on the filling ratio. The unit price of paraffin is typically 10 yuan/kg, while metal foam costs approximately 30,000 yuan/m^3. The welding cost of metal foam constitutes the majority of the installation cost, estimated to be 10% of the material cost of metal foam, while the installation cost of other parts is negligible.

$$I = I_m + I_w \tag{15}$$

where I_m is the material cost (yuan, equal to 20 yuan plus the purchase cost of paraffin and metal foam); I_w represents the installation cost (yuan, equal to the total price of the metal foam multiplied by 10%).

Fig. 7 depicts the cost of a single TES unit as a function of its filling ratio. As the filling ratio is decreased from 100% to 60%, the purchase cost of paraffin rises by a nominal 0.4 yuan, whereas the cost of metal foam experiences a considerable reduction of 19.4 yuan. Consequently, the overall cost of a TES unit decreases from 85.4 yuan to 64.4 yuan. If the TES unit is devoid of metal foam, the single cost is merely 32.9 yuan. In addition to the initial one-time capital investment mentioned above, the phase change heat storage system requires a continuous power supply to facilitate the circulation of the HTF using equipment such as a water pump. The pressure loss, ΔP, in the regenerative heating water system pipe arises due to both frictional resistance loss and local resistance loss. The frictional resistance loss is further divided into two parts, namely the heat transfer pipe and the heat exchange pipe, which can be calculated using the following equations:

$$\Delta P = \lambda_1 \frac{l_1}{D_1} \frac{\rho_{水} v_1^2}{2} + \lambda_2 \frac{l_2}{D_2} \frac{\rho_{水} v_2^2}{2} + \Delta P_j \tag{16}$$

where λ, l, D and ρ_{water} donate the friction factor of the pipe, the pipe length (m), the pipe diameter (m) and the density of water at 70 °C (977.759 kg m^{-3}), respectively; v is the HTF velocity ($m{\cdot}s^{-1}$); the subscripts 1 and 2 represent the heat transfer pipe and the heat exchange pipe respectively. ΔP_j (local resistance loss) is estimated as a percentage of frictional resistance loss, taking 20% when the pipe is longer and 40% when the pipe is shorter. The length of the heat exchange pipe is 0.3 m, the pipe diameter is 0.02 m, the flow rate is 0.04 m s^{-1}, and $Re < 2300$ can be calculated, which is laminar flow, $\lambda_2 = 64/Re$. The local resistance loss in turbulent transition zone of the tube is calculated by the following empirical equation:

$$\frac{1}{\sqrt{\lambda_1}} = -2\lg\left(\frac{\kappa}{3.7D_1} + \frac{2.51}{\mathrm{Re}\sqrt{\lambda_1}}\right) \tag{17}$$

where κ is the equivalent absolute roughness on the surface of the pipe (m, take 0.2 mm closed circulating water system).

All pipeline resistance losses are converted from Pa to mH_2O and the potential height difference between the heat source and the heating terminal is added to obtain the total head. The specific pump model and motor power G can be determined by considering a 10% surplus of flow and head during the pump selection process. The operating cost F of the TES system is estimated by calculating the electricity charge based on the current domestic electricity price segment in Shaanxi Province, which is 0.4983 yuan/kWh. It takes the form of

$$F = 0.4983HG \tag{18}$$

where F defines the daily operating cost of the TES system (yuan); H represents the daily running time of the TES (h); G is the shaft power of the shaft (kW).

Assuming that the thermal energy of the HTF in the TES system is generated through solar power, the duration of sunlight in winter in Xi'an over the past decade (2011–2021) was obtained from the China Statistical Yearbook. Based on an average of December, January, and February, the average daily sunlight duration in Xi'an during winter was calculated to be 4 h. Consequently, the heat

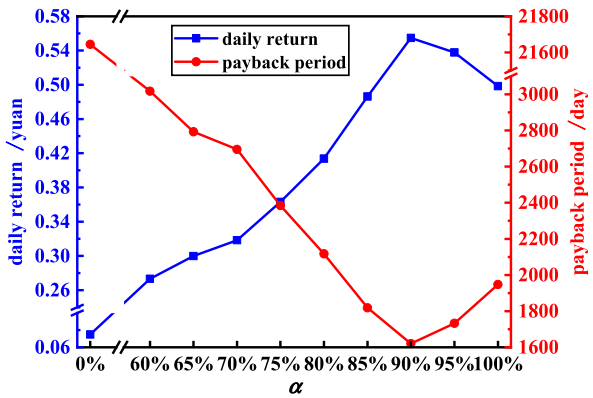

Fig. 8. Daily return and payback period for the small heat storage system.

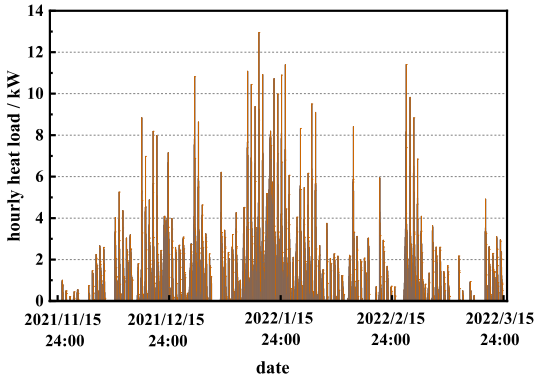

(a) Hourly heat load of the office building in winter

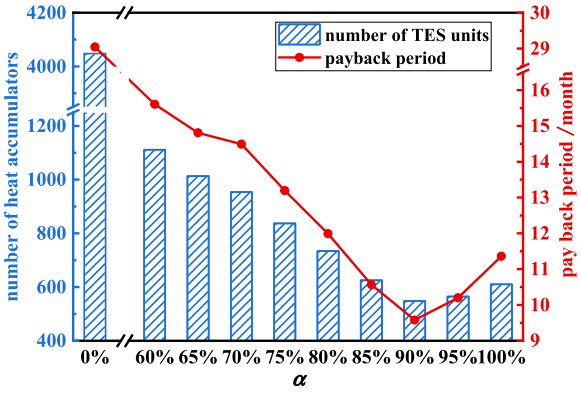

(b) The number of TES units required for the office heating and the payback period

Fig. 9. Hourly heat load and economic benefits of the office building.

storage duration of the system is 4 h per day during the heating season. If a small phase change TES system consists of ten parallel shell-and-tube TES units, and the flow rate of HTF in one heat storage branch pipe is 0.045 $m^3\ h^{-1}$, the total design flow rate of the heat transport main pipe is 0.45 $m^3\ h^{-1}$.

The flow rate, diameter, and length of the heat pipe are 0.4 m s^{-1}, 0.02 m, and 10 m, respectively. The total resistance loss of the pipe was determined to be 2234.75 Pa using Eqs. (15) and (16). In addition, the pump head required was calculated to be 3.53 m, accounting for the height difference of 3.3 m. The Self-priming centrifugal pump 16WFB1-A, with a shaft power of 0.03 kW, was selected. Based on Eq. (17), the estimated daily operational cost is 0.06 yuan. The cost is minimally impacted by the metal foam filling ratio in the phase change accumulator and increases with the rise of pipe network flow and head.

4.3.2. Calculation of return and payback period

According to the complete melting time under different filling ratios. Under ideal condition, the volume V of PCM for heat storage in ideal condition is defined as:

$$V = \frac{3600H}{t_{\text{full}}} \times \pi\left(R^2 - r^2\right)h \times (1 - \alpha + \alpha\varepsilon) \tag{19}$$

where, t_{full} defines the time required by a TES unit for complete heat storage at one time/s; R, r, h, α *and* ε respectively account for the radius of the TES tank (m), the radius of the heat exchange pipe (m), the height of the TES tank (m), metal foam filling ratio (%) and metal foam porosity.

The heat stored by PCMs includes latent heat and apparent heat.

$$Q = \rho_{\text{f}} V \times \left[L + c_{pf}\left(T_{\text{af}} - T_0\right)\right] \tag{20}$$

where ρ_{f}, L and c_{pf} separately exhibit the density of paraffin (800 kg m^{-3}), the latent heat of paraffin (200 kJ kg^{-1}) and the specific heat

capacity of paraffin (2 kJ kg^{-1} K^{-1}); T_{af} represents the mean temperature of paraffin at the complete melting time (K); T_0 is the initial temperature of the PCM (K).

According to the heat price of 0.21 yuan/kWh for non-resident in Xi 'an, the daily return E of the phase change TES system can be estimated when the stored heat is used for heating.

$$E = 0.21N\frac{Q}{3600} \tag{21}$$

where N donates the number of the TES units; Q is the total heat stored per day by a TES unit (kJ).

According to Eqs. (19)–(21), the initial investment, operating cost and daily return of the TES system are obtained, and the payback period P_t is calculated as follows:

$$P_t = \frac{NI}{E - F} \tag{22}$$

where P_t is the profit return time (days); *I, E and F* define the cost of a TES unit (yuan), the daily return (yuan) of the TES system and the daily operation cost of the TES system (yuan), respectively.

In the preceding section, the operational cost of a small TES system consisting of 10 TES units was illustrated. Based on the results, an estimation of the daily return and payback period of the system was conducted, as depicted in Fig. 8. The figure highlights that in the absence of metal foam filling, the melting rate is significantly slow, and only around 1/3 of the heat storage process can be accomplished within 4 h. This results in a daily return of merely 0.075 yuan and a payback period of roughly 59.3 years, which is not a feasible option for construction and operation. In comparison, a metal foam filling ratio of 90% yields the highest returns per day, which is an 11.3% increase over the returns obtained with 100% filling ratio. It appears that when the metal foam filling ratio decreases to 85% or below, there is a reduction in the daily return compared to the 100% filling ratio. Moreover, when the filling ratio drops to 82% or below, there is an increase in the payback period compared to the 100% filling ratio. It is evident that the addition of metal foam significantly enhances the daily thermal energy storage and expected returns, thereby shortening the payback period to an acceptable range.

4.3.3. *Economic benefits of the heating building*

Fig. 9(a) depicts the hourly heat load of the office building throughout the heating period. The heat load experiences significant variations between working days and holidays, and sharp fluctuations are observed between day and night. The maximum heat load of 12.95 kW is recorded at 8 a.m. on January 9, over the entire heating period from November 15th to March 15th. By combining this with the office building's area, the heat index is calculated to be 23.2 W m^{-2}. The maximum daily total heat consumption of the office building is 144.57 kWh, which occurs on January 12th and is used as a basis for selecting the phase change heat storage heating system. Based on the simulation results, the total heating heat consumption of the office building is estimated to be 3108.41 kWh over the entire heating period.

According to the heat load and the heat storage capacity of the accumulator with different filling ratio, the required number of Thermal Energy Storage (TES) units is calculated. This information is then used to determine the initial investment by multiplying the number of TES units with their respective unit prices. To calculate the daily operating cost of the heating system, Eq. (18) is utilized, where the power of the pump shaft is substituted with the total power consumption. The total power consumption is estimated by:

$$G = \frac{0.004225Q(17 + 0.0115l_1)}{\Delta T} \tag{23}$$

where G represents the power consumption of heating system (kWh); Q is the design heat load (144.57 kWh); l_1 accounts for the total length of water supply and return pipe (400 m); ΔT donates the design return water temperature (20 °C).

Energy-saving design standards for public buildings stipulate the maximum allowable values for power consumption and heat transfer ratio. If the office building uses a primary pump system, the maximum designed flow of the pump should not exceed 60 m^3 h^{-1}. Based on this, the daily operating cost is estimated to be around 0.33 yuan. Eq. (23) demonstrates that the operating cost of the heating system increases with an increase in heat load and pipe network function radius, while it decreases with an increase in the temperature difference between the supply and return water.

According to the heating price of non-resident buildings in Xi 'an (7.5 yuan/month m^2), and accounting for the conversion coefficient of buildings over 3 m in height, we estimate that the monthly central heating cost for this office building without utilizing phase transition heat storage heating would be 4597.56 yuan. When compared with the central heating scheme, the initial investment cost of the phase change heat storage scheme is relatively high, while the electricity cost of the water pump during operation is relatively low. Therefore, the payback period of a building heating engineering case is defined as the point in time where the total cost of the heat storage scheme, including the initial investment and total operating cost, is equivalent to the total cost of the heating scheme.

To effectively quantify the economic indicators of partially-filled TES units applied to heating, we present a bar chart and dot plot in Fig. 9(b). The bar chart displays the required number of TES units, while the dot plot illustrates the payback period under different metal foam filling ratios. As the filling ratio decreases from 100% to 60%, both indicators display a decreasing first but then increasing trend, which is consistent with the time required for complete melting of the PCM.

To meet the daily heating load of the building without filling the TES units with metal foam, a total of 4048 TES units are required. Although the cost of each TES unit is relatively low, the high number of units required significantly increases the total initial

investment, resulting in a payback period of 29 months. However, as shown in Fig. 9(b), a horizontal filling ratio of 90% in the metal foam leads to a complete melting time of 5310 s and a reduced number of required TES units. In this case, only 548 TES units are necessary to meet the heating load, demonstrating the potential of partially-filled metal foam structures in reducing initial investment and equipment size while improving energy efficiency and reducing emissions. Furthermore, considering that the heating season in Xi'an lasts only four months per year, the partially-filled 90% metal foam heat storage system would pay for itself in just three heating seasons, highlighting the exceptional economic viability of this approach.

5. Conclusions

This paper presents a simulation of the melting process to evaluate the thermal characteristics of a metal foam horizontal partially filled shell-and-tube TES system. In addition, the economic benefits of the system are calculated, including initial investment, operating costs, daily return, and payback period, under varying filling ratios. The economic feasibility of the system is also assessed in the context of building heating scenarios.

Based on the analysis, we can draw the following conclusions.

(1) The analysis indicates that the heat storage efficiency of the system without metal foam filling is exceedingly low and fails to meet the desired heat storage requirements within the specified time. However, the introduction of a horizontal partially filled metal foam structure significantly improves heat transfer rates. For instance, the TES unit with a filling ratio of 90% achieves a complete melting time of 5310 s, which is 87.56% shorter than that of the TES unit with pure PCM. This underscores the critical role of metal foam structures in enhancing the heat transfer capacity of TES systems, and the horizontal filling structure with 90% filling ratio has better performance in the application.

(2) As the metal foam filling ratio decreases, the quantity of the relatively expensive metal foam reduces, resulting in a noticeable decrease in initial investment costs. For small-scale TES systems comprising ten TES units, the daily returns initially increase and then decrease with decreasing filling ratios. Similarly, the payback period initially reduces, but then extends as the filling ratio decreases. Comparably, a metal foam filling ratio of 90% yields the highest daily returns and shortest payback period. These findings highlight the complex interplay between metal foam filling ratios, initial investment costs, daily returns, and payback periods, which must be carefully considered for cost-effective TES system design and implementation.

(3) When meeting the heating load requirements of an office building in Xi'an during winter, the horizontal partially filled TES units with a filling ratio of 90% demonstrate the lowest number of required units, totaling 548. The payback period for this configuration is shortest, about three heating seasons. These results suggest that the partially filled structure with a 90% filling ratio can achieve a balance between heat storage efficiency and economic benefits, resulting in a mutually beneficial outcome. Consequently, this configuration (90% filling ratio) is a promising option for designing and implementing cost-effective TES systems in similar regions for practical engineering application.

Author statement

Xinyu Gao: Software, Data Curation, Validation, Formal analysis, Visualization, Methodology, Writing (Original Draft, Review & Editing).

Zhaoyang Niu: Investigation, Methodology, Software, Data Curation, Formal analysis.

Xinyu Huang: Methodology, Data Curation, Formal analysis.

Xiaohu Yang: Conceptualization, Resources, Methodology, Supervision, Writing (Original Draft, Review & Editing).

Jinyue Yan: Conceptualization, Data Curation, Proofreading, Writing (Review & Editing).

Declaration of competing interest

The authors declare that they have no known competing financial interests or personal relationships that could have appeared to influence the work reported in this paper.

Data availability

No data was used for the research described in the article.

Acknowledgements

This work was supported by the Key Scientific and Technological Innovation Team of Shaanxi Province (2023-CX-TD-29). Xiaohu Yang gratefully acknowledges the support of K. C. Wong Education Foundation.

References

[1] L. Lundstrom, F. Wallin, Heat demand profiles of energy conservation measures in buildings and their impact on a district heating system, Appl. Energy 161 (2016) 290–299.

[2] H.F. Chen, J. Ji, G. Pei, J. Yang, Y. Zhang, Experimental and numerical comparative investigation on a concentrating photovoltaic system, J. Clean. Prod. 174 (2018) 1288–1298.

[3] H.F. Chen, Y.J. Wang, J. Li, B.R. Cai, F.W. Zhang, T. Lu, J. Yang, L.L. Jiang, Y. Zhang, J.Z. Zhou, Experimental research on a solar air-source heat pump system with phase change energy storage, Energy Build. 228 (2020), 110451.

[4] A. de Gracia, L.F. Cabeza, Phase change materials and thermal energy storage for buildings, Energy Build. 103 (2015) 414–419.
[5] H. Nazir, M. Batool, F.J.B. Osorio, M. Isaza-Ruiz, X.H. Xu, K. Vignarooban, P. Phelan, Inamuddin, A.M. Kannan, Recent developments in phase change materials for energy storage applications: a review, Int. J. Heat Mass Tran. 129 (2019) 491–523.
[6] H.M. Teamah, M.F. Lightstone, J.S. Cotton, An alternative approach for assessing the benefit of phase change materials in solar domestic hot water systems, Sol. Energy 158 (2017) 875–888.
[7] Z.L. Wang, H. Zhang, B.L. Dou, G.H. Zhang, W.D. Wu, Influence of inlet structure on thermal stratification in a heat storage tank with PCMs: CFD and experimental study, Appl. Therm. Eng. 162 (2019), 114151.
[8] J. Xu, R.Z. Wang, Y. Li, A review of available technologies for seasonal thermal energy storage, Sol. Energy 103 (2014) 610–638.
[9] S.S. Anandan, J. Sundarababu, A Comprehensive Review on Mobilized Thermal Energy Storage, Energ Source Part A, 2021, pp. 1–24.
[10] E. Guelpa, V. Verda, Thermal energy storage in district heating and cooling systems: a review, Appl. Energy 252 (2019), 113474.
[11] C.R. Matos, J.F. Carneiro, P.P. Silva, Overview of large-scale underground energy storage technologies for integration of renewable energies and criteria for reservoir identification, J. Energy Storage 21 (2019) 241–258.
[12] H.L. Zhang, J. Baeyens, J. Degreve, G. Caceres, R. Segal, F. Pitie, Latent heat storage with tubular-encapsulated phase change materials (PCMs), Energy 76 (2014) 66–72.
[13] J. Zhao, J.M. Gao, J.H. Liao, B.T. Zhou, Y.F. Bai, T.W. Qiang, An experimental study of the heat storage and the discharge performance and an economic performance analysis of a flat plate phase change material (PCM) storage tank, Energies 15 (2022) 4023.
[14] M. Yang, Z.F. Wang, J.F. Yang, G.F. Yuan, W.S. Wang, W.H. Shi, Thermo-economic analysis of solar heating plant with the seasonal thermal storage in Northern China, Sol. Energy 232 (2022) 212–231.
[15] H.M. Ushamah, N. Ahmed, K.E. Elfeky, M. Mahmood, M.A. Qaisrani, A. Waqas, Q. Zhang, Techno-economic analysis of a hybrid district heating with borehole thermal storage for various solar collectors and climate zones in Pakistan, Renew. Energy 199 (2022) 1639–1656.
[16] A.A. Mathew, V. Thangavel, A novel thermal storage integrated evacuated tube heat pipe solar air heater: energy, exergy, economic and environmental impact analysis, Sol. Energy 220 (2021) 828–842.
[17] Y.X. Zhang, B.H. Lu, Z.X. Wang, J.J. Zhu, J.Y. Zhang, C. Wang, Experimental investigation on the charging and discharging performance enhancement of a vertical latent heat thermal energy storage unit via snowflake fin design, Int. J. Heat Mass Tran. 199 (2022), 123455.
[18] P. Ping, R.Q. Peng, D.P. Kong, G.M. Chen, J. Wen, Investigation on thermal management performance of PCM-fin structure for Li-ion battery module in high-temperature environment, Energy Convers. Manag. 176 (2018) 131–146.
[19] M. Gurturk, B. Kok, A new approach in the design of heat transfer fin for melting and solidification of PCM, Int. J. Heat Mass Tran. 153 (2020), 119671.
[20] J.F. Guo, X.Y. Wang, B. Yang, X.H. Yang, M.J. Li, Thermal assessment on solid-liquid energy storage tube packed with non-uniform angled fins, Sol. Energy Mater. Sol. Cell. 236 (2022), 111526.
[21] F.L. Rashid, A. Hadi, N.H. Al-Garah, A. Hashim, Novel phase change materials, MgO nanoparticles, and water based nanofluids for thermal energy storage and biomedical applications, Int J Pharm Phytopha 8 (2018) 46–56.
[22] S.P. Mo, K.D. Zhu, T. Yin, Y. Chen, Z.D. Cheng, Phase change characteristics of ethylene glycol solution-based nanofluids for subzero thermal energy storage, Int. J. Energy Res. 41 (2017) 81–91.
[23] Y. Maleki, M. Mehrpooya, F. Pourfayaz, Cold thermal energy storage by encapsulated phase change materials system using hybrid nanofluids as the heat transfer fluid, Int. J. Energy Res. 45 (2021) 15265–15283.
[24] K.R. Kondakrindi, M.R. Reddigari, B.D. Prasad, Experimental investigation on the influence of nanofluids used as heat transfer fluid in phase change material based thermal energy storage system, Therm. Sci. 25 (2021) 643–652.
[25] Q.Q. Zhang, Z.C. Sun, Q.W. Guo, Y. Zhou, Z.Z. Li, J.Y. Wen, F.R. Li, Y.Y. Liu, S.Z. Jiao, Construction of excellent visible light absorption heat storage slurry using phase change microcapsules for solar thermal utilization, ChemistrySelect 7 (2022), e202202124.
[26] J.T. Wu, Y.J. Zhang, K.L. Sun, Q.C. Chen, Heat transfer enhancement of phase change material in triple-tube latent heat thermal energy storage units: operating modes and fin configurations, Energies 15 (2022) 5653.
[27] A.U. Rehman, S.R. Sheikh, Z. Kausar, M. Grimes, S.J. McCormack, Experimental thermal response study of multilayered, encapsulated, PCM-integrated building construction materials, Energies 15 (2022) 6356.
[28] B. Palmer, A. Arshad, Y. Yang, C. Wen, Energy storage performance improvement of phase change materials-based triplex-tube heat exchanger (TTHX) using liquid-solid interface-informed fin configurations, Appl. Energy 333 (2023), 120576.
[29] T.M.O. Diallo, M. Yu, J.Z. Zhou, X.D. Zhao, S. Shittu, G.Q. Li, J. Ji, D. Hardy, Energy performance analysis of a novel solar PVT loop heat pipe employing a microchannel heat pipe evaporator and a PCM triple heat exchanger, Energy 167 (2019) 866–888.
[30] H. Behi, D. Karimi, F.H. Gandoman, M. Akbarzadeh, S. Khaleghi, T. Kalogiannis, M.S. Hosen, J. Jaguemont, J. Van Mierlo, M. Berecibar, PCM assisted heat pipe cooling system for the thermal management of an LTO cell for high-current profiles, Case Stud. Therm. Eng. 25 (2021), 100920.
[31] F.F. Li, X.Y. Huang, Y.J. Li, L. Lu, X.Z. Meng, X.H. Yang, B. Sunden, Application and analysis of flip mechanism in the melting process of a triplex-tube latent heat energy storage unit, Energy Rep. 9 (2023) 3989–4004.
[32] Z. Du, G. Liu, X.Y. Huang, T. Xiao, X.H. Yang, Y.L. He, Numerical studies on a fin-foam composite structure towards improving melting phase change, Int. J. Heat Mass Tran. 208 (2023), 124076.
[33] G. Liu, Z. Du, T. Xiao, J.F. Guo, L. Lu, X.H. Yang, K. Hooman, Design and assessments on a hybrid pin fin-metal foam structure towards enhancing melting heat transfer: an experimental study, Int. J. Heat Mass Tran. 182 (2022), 107809.
[34] H. Walter, A. Beck, M. Hameter, Transient analysis of an improved finned tube heat exchanger for thermal energy storage system, in: Proc. Asme 9th Int. Conf. Energy Sustain 2, 2015, V002T13A003 (2016).
[35] Z.Q. Zhu, Y.K. Huang, N. Hu, Y. Zeng, L.W. Fan, Transient performance of a PCM-based heat sink with a partially filled metal foam: effects of the filling height ratio, Appl. Therm. Eng. 128 (2018) 966–972.
[36] S. Rahmanian, M. Moein-Jahromi, H. Rahmanian-Koushkaki, K. Sopian, Performance investigation of inclined CPV system with composites of PCM, metal foam and nanoparticles, Sol. Energy 230 (2021) 883–901.
[37] M.M. Heyhat, S. Mousavi, M. Siavashi, Battery thermal management with thermal energy storage composites of PCM, metal foam, fin and nanoparticle, J. Energy Storage 28 (2020), 101235.
[38] A. Alhusseny, N. Al-Zurfi, A. Nasser, A. Al-Fatlawi, M. Aljanabi, Impact of using a PCM-metal foam composite on charging/discharging process of bundled-tube LHTES units, Int. J. Heat Mass Tran. 150 (2020), 119320.
[39] M.M. El Idi, M. Karkri, Heating and cooling conditions effects on the kinetic of phase change of PCM embedded in metal foam, Case Stud. Therm. Eng. 21 (2020), 100716.
[40] X. Meng, L.Y. Yan, J.Q. Xu, F. He, H.T. Yu, M. Zhang, Effect of porosity and pore density of copper foam on thermal performance of the paraffin-copper foam composite Phase-Change Material, Case Stud. Therm. Eng. 22 (2020), 100742.
[41] T. Xiao, G. Liu, J.F. Guo, G. Shu, L. Lu, X.H. Yang, Effect of metal foam on improving solid-liquid phase change in a multi-channel thermal storage tank, Sustain Energy Techn 53 (2022), 102533.
[42] T. Xiao, X.H. Yang, K. Hooman, T.J. Lu, Analytical fractal models for permeability and conductivity of open-cell metallic foams, Int. J. Heat Mass Tran. 177 (2021), 121509.
[43] G. Liu, T. Xiao, J.F. Guo, P. Wei, X.H. Yang, K. Hooman, Melting and solidification of phase change materials in metal foam filled thermal energy storage tank: evaluation on gradient in pore structure, Appl. Therm. Eng. 212 (2022), 118564.
[44] Y.T. Huo, Y.Q. Guo, Z.H. Rao, Investigation on the thermal performance of phase change material/porous medium-based battery thermal management in pore scale, Int. J. Energy Res. 43 (2019) 767–778.
[45] M. Esapour, A. Hamzehnezhad, A.A.R. Darzi, M. Jourabian, Melting and solidification of PCM embedded in porous metal foam in horizontal multi-tube heat storage system, Energy Convers. Manag. 171 (2018) 398–410.

[46] B.V.S. Dinesh, A. Bhattacharya, Effect of foam geometry on heat absorption characteristics of PCM-metal foam composite thermal energy storage systems, Int. J. Heat Mass Tran. 134 (2019) 866–883.
[47] S. Sivasankaran, F.O.M. Mallawi, Numerical study on convective flow boiling of nanoliquid inside a pipe filling with aluminum metal foam by two-phase model, Case Stud. Therm. Eng. 26 (2021), 101095.
[48] H. Peng, M.L. Li, F.F. Hu, S.Y. Feng, Performance analysis of absorber tube in parabolic trough solar collector inserted with semi-annular and fin shape metal foam hybrid structure, Case Stud. Therm. Eng. 26 (2021), 101112.
[49] C. Ding, L. Wang, Z.L. Niu, Thermal performance evaluation of latent heat storage systems with plate fin-metal foam hybrid structure, Case Stud. Therm. Eng. 27 (2021), 101309.
[50] Z.Q. Zhang, X.D. He, Three-dimensional numerical study on solid-liquid phase change within open-celled aluminum foam with porosity gradient, Appl. Therm. Eng. 113 (2017) 298–308.
[51] A.R. Karimi, M. Siavashi, M. Tahmasbi, A.M. Norouzi, Experimental analysis to improve charge/discharge of thermal energy storage in phase change materials using helical coil and porous metal foam, J. Energy Storage 55 (2022), 105759.
[52] B. Wang, J. Xue, Z. Du, J. Yu, L. Lu, T. Xiao, X. Yang, Numerical Optimization Design of Heat Storage Tank with Metal Foam for Enhancing Phase Transition, J Taiwan Inst Chem E, 2022, 104644.
[53] M. Shirbani, M. Siavashi, M. Bidabadi, Phase change materials energy storage enhancement schemes and implementing the lattice Boltzmann method for simulations: a review, Energies 16 (2023) 1059.
[54] R. Paknahad, M. Siavashi, M. Hosseini, Pore-scale fluid flow and conjugate heat transfer study in high porosity Voronoi metal foams using multi-relaxation-time regularized lattice Boltzmann (MRT-RLB) method, Int. Commun. Heat Mass Tran. 141 (2023), 106607.
[55] X. Hu, X. Gong, Pore-scale numerical simulation of the thermal performance for phase change material embedded in metal foam with cubic periodic cell structure, Appl. Therm. Eng. 151 (2019) 231–239.
[56] A. Žukauskas, Heat transfer from tubes in crossflow, in: J.P. Hartnett, T.F. Irvine (Eds.), Adv. Heat Tran. 8 (1972) 93–160.
[57] X.H. Yang, J.X. Bai, H.B. Yan, J.J. Kuang, T.J. Lu, T. Kim, An analytical unit cell model for the effective thermal conductivity of high porosity open-cell metal foams, Transport Porous Media 102 (2014) 403–426.
[58] J.G. Georgiadis, I. Catton, Dispersion in cellular thermal-convection in porous layers, Int. J. Heat Mass Tran. 31 (1988) 1081–1091.
[59] A. Bhattacharya, V.V. Calmidi, R.L. Mahajan, Thermophysical properties of high porosity metal foams, Int. J. Heat Mass Tran. 45 (2002) 1017–1031.
[60] J.G. Fourie, J.P. Du Plessis, Pressure drop modelling in cellular metallic foams, Chem. Eng. Sci. 57 (2002) 2781–2789.